

# Structure-preserving Sparse Identification of Nonlinear Dynamics for Data-driven Modeling

Kookjin Lee<sup>1</sup>, Nathaniel Trask<sup>2</sup>, and Panos Stinis<sup>3</sup>

<sup>1</sup> School of Computing and Augmented Intelligence, Arizona State University, Tempe, AZ 85281

<sup>2</sup> Center for Computing Research, Sandia National Laboratories, Albuquerque, NM 87123

<sup>3</sup> Pacific Northwest National Laboratory, Richland, WA 99354

kookjin.lee@asu.edu, natrask@sandia.gov, panagiotis.stinis@pnnl.gov

## Abstract

Discovery of dynamical systems from data forms the foundation for data-driven modeling and recently, structure-preserving geometric perspectives have been shown to provide improved forecasting, stability, and physical realizability guarantees. We present here a unification of the Sparse Identification of Nonlinear Dynamics (SINDy) formalism with neural ordinary differential equations. The resulting framework allows learning of both "black-box" dynamics and learning of structure preserving bracket formalisms for both reversible and irreversible dynamics. We present a suite of benchmarks demonstrating effectiveness and structure preservation, including for chaotic systems.

## Introduction

A number of scientific machine learning (ML) tasks seek to discover a dynamical system whose solution is consistent with data (e.g. constitutive modeling (Patel et al. 2020; Karapiperis et al. 2021; Ghnatios et al. 2019; Masi et al. 2021), reduced-order modeling (Chen et al. 2021; Lee and Carlberg 2021; Wan et al. 2018), physics-informed machine learning (Karniadakis et al. 2021; Wu, Xiao, and Paterson 2018), and surrogates for performing optimal control (Alexopoulos, Nikolakis, and Chryssoulouris 2020)). A major challenge for this class of problems is the preservation of both numerical stability and physical realizability when performing out of distribution inference (i.e. extrapolation/forecasting). Unlike traditional ML for e.g. image/language processing tasks, engineering and science models pose strict requirements on physical quantities to guarantee properties such as conservation, thermodynamic consistency and well-posedness of resulting models (Baker et al. 2019). These structural constraints translate to desirable mathematical properties for simulation, such as improved numerical stability and accuracy, particularly for chaotic systems (Lee, Trask, and Stinis 2021; Trask, Huang, and Hu 2020).

While so-called physics-informed ML (PIML) approaches seek to impose these properties by imposing soft physics constraints into the ML process, many applications require structure preservation to hold exactly; PIML requires empirical tuning of weighting parameters and physics properties hold only to within optimization error, which typically may be large (Wang, Teng, and Perdikaris 2020; Rohrhofer, Posch, and Geiger 2021). Structure-preserving

machine learning has emerged as a means of designing architectures such that physics constraints hold exactly by construction (Lee, Trask, and Stinis 2021; Trask, Huang, and Hu 2020). By parameterizing relevant geometric or topological structures, researchers obtain more data-efficient hybrid physics/ML architectures with guaranteed mathematical properties.

In this work we consider geometric structure preservation for dynamical systems (Hairer et al. 2006; Marsden and Ratiu 1995). Reversible bracket formalisms (e.g. Hamiltonian/Lagrangian mechanics) have been shown effective for learning reversible dynamics (Toth et al. 2019; Cranmer et al. 2020; Lutter, Ritter, and Peters 2018; Chen et al. 2019; Jin et al. 2020; Tong et al. 2021; Zhong, Dey, and Chakraborty 2021; Chen and Tao 2021; Bertalan et al. 2019), while dissipative metric bracket extensions provide generalizations to irreversible dynamics in the metriplectic formalism (Lee, Trask, and Stinis 2021; Desai et al. 2021; Hernández et al. 2021; Yu et al. 2020; Zhong, Dey, and Chakraborty 2020). Accounting for dissipation in this manner provides important thermodynamic consistency guarantees: namely, discrete versions of the first and second law of thermodynamics along with a fluctuation-dissipation theorem for thermal systems at microscales. Training these models is however a challenge and leads to discovery of non-interpretable *Casimirs* (generalized entropy and energy functionals describing the system).

For  $\mathbf{x}(t) \in \mathbb{R}^n$  denoting the state of a system at time  $t$ ,  $\mathbf{f}$  denoting a velocity with potentially exploitable mathematical structure, and  $\Theta$  denoting trainable parameters, we consider learning of dynamics of the form

$$\frac{d\mathbf{x}(t)}{dt} = \mathbf{f}_{\Theta}(\mathbf{x}).$$

We synthesize the Sparse Identification of Nonlinear Dynamics (SINDy) formalism (Brunton, Proctor, and Kutz 2016) with neural ordinary differential equations (NODEs) (Chen et al. 2018) to obtain a framework for learning dynamics. This sparse dictionary-learning formalism allows learning of either interpretable  $\mathbf{f}$  when learning "black-box" ODEs, or for learning more complicated bracket dynamics for  $\mathbf{f}$  which describe structure-preserving reversible and irreversible systems. Our main technical contributions include:

- a novel extension of SINDy into neural ODE settings, including a training strategy with L1 weight decay and pruning,
- the first application of SINDy with structure-preservation, including: black-box, Hamiltonian, GENERIC, and port-Hamiltonian formulations
- empirical demonstration on the effectiveness of the proposed algorithm for a wide array of dynamics spanning: reversible, irreversible, and chaotic systems.

## Sparse Identification of Nonlinear Dynamics (SINDy)

The Sparse Identification of Nonlinear Dynamics (SINDy) method aims to identify the dynamics of interest using a sparse set of dictionaries such that

$$\mathbf{f}_\Theta(\mathbf{x}) = (\boldsymbol{\phi}(\mathbf{x})^\top \Xi)^\top,$$

where  $\Xi \in \mathbb{R}^{p \times n}$  is the coefficient matrix and  $\boldsymbol{\phi}(\mathbf{z}) \in \mathbb{R}^{1 \times p}$  denotes a ‘‘library’’ vector consisting of candidate functions, e.g., constant, polynomials, and so on.

From measurements of states (and derivatives), we can construct a linear system of equations:

$$\dot{X} = \Phi(X)\Xi$$

where  $X \in \mathbb{R}^{m \times n}$  and  $\dot{X} \in \mathbb{R}^{m \times n}$  are collections of the states  $\mathbf{x}(t)$  and the (numerically approximated) derivatives  $\frac{d\mathbf{x}}{dt}$  sampled at time indices  $\{t_1, \dots, t_m\}$  such that

$$[X]_{ij} = x_j(t_i), \quad \text{and} \quad [\dot{X}]_{ij} = \frac{dx_j}{dt}(t_i).$$

A library,  $\Phi(X) \in \mathbb{R}^{m \times p}$ , consists of candidate nonlinear functions, e.g., constant, polynomial, and trigonometric terms:

$$\Phi(X) = [\mathbb{1} \quad X \quad \mathbb{P}_2(X) \quad \dots \quad \cos(X) \quad \dots],$$

where  $\mathbb{P}_2$  is a function of the quadratic nonlinearities such that the  $i$ th row of  $\mathbb{P}_2(X)$  is defined as, for example, with  $n = 3$ ,

$$[\mathbb{P}_2(X)]_i^\top = [x_1^2(t_i), x_1(t_i)x_2(t_i), x_1(t_i)x_3(t_i), x_2^2(t_i), x_2(t_i)x_3(t_i), x_3^2(t_i)].$$

Lastly,  $\Xi \in \mathbb{R}^{p \times n}$  denotes the collection of the unknown coefficients  $\Xi = [\xi_1, \dots, \xi_n]$ , where  $\xi_i \in \mathbb{R}^p$ ,  $i = 1, \dots, n$  are sparse vectors.

Typically, only  $X$  is available and  $\dot{X}$  is approximated numerically. Thus, in SINDy,  $\dot{X}$  is considered to be noisy, which leads to a new formulation:

$$\dot{X} = \Phi(X)\Xi + \eta Z,$$

where  $Z$  is a matrix of independent identically distributed unit normal entries and  $\eta$  is noise magnitude. To compute the sparse solution  $\Xi$ , SINDy employs either the least absolute shrinkage and selection operator (LASSO) (Tibshirani 1996) or sequential threshold least-squares method (Brunton, Proctor, and Kutz 2016). LASSO is an L1-regularized regression technique and the sequential threshold least-squares method is an iterative algorithm which repetitively zeroes out entries of  $\Xi$  and solves least-squares problems with remaining entries of  $\Xi$ .

## Neural SINDy

One evident weakness of SINDy is that it requires the derivatives of the state variable either empirically measured or numerically computed. To resolve this issue, we propose to use the training algorithm introduced in neural ordinary differential equations (NODEs) (Chen et al. 2018) with L1 weight decay. In addition, we propose the magnitude-based pruning strategy to retain only the dictionaries with significant contributions.

## Neural Ordinary Differential Equations

NODEs (Chen et al. 2018) are a family of deep neural network models that parameterize the time-continuous dynamics of hidden states  $\mathbf{z}(t)$  using a system of ODEs:

$$\frac{d\mathbf{z}(t)}{dt} = \mathbf{f}_\Theta(\mathbf{z}, t),$$

where  $\mathbf{z}(t)$  is a time-continuous representation of a state,  $\mathbf{f}_\Theta$  is a parameterized (trainable) velocity function, and  $\Theta$  is a set of neural network weights and biases.

In the forward pass, given the initial condition  $\mathbf{z}(0)$ , a hidden state at any time index can be obtained by solving the initial value problem (IVP). A black-box time integrator can be employed to compute the hidden states with the desired accuracy:

$$\tilde{\mathbf{z}}(t_1), \dots, \tilde{\mathbf{z}}(t_m) = \text{ODESolve}(\mathbf{z}(0), \mathbf{f}_\Theta, t_1, \dots, t_m).$$

The model parameters  $\Theta$  are then updated with an optimizer, which minimizes a loss function measuring the difference between the output and the target variables.

**Dictionary-based parameterization** As in the original SINDy formulation, we assume that there is a set of candidate nonlinear functions to represent the dynamics

$$\mathbf{f}_\Theta(\mathbf{z}) = (\boldsymbol{\phi}(\mathbf{z})^\top \Xi)^\top, \quad (1)$$

where, again,  $\Xi \in \mathbb{R}^{p \times n}$  is a trainable coefficient matrix and  $\boldsymbol{\phi}(\mathbf{z}) \in \mathbb{R}^{1 \times p}$  denotes a library vector. In this setting, the learnable parameters of NODE become  $\Theta = \Xi$ .

**Sparsity inducing loss: L1 weight decay (Lasso)** Following SINDy, to induce sparsity in  $\Xi$  we add an L1 weight decay to the main loss objective for the mean absolute error:

$$\mathcal{L} = \frac{1}{n_{\text{train}}} \sum_{\ell=1}^{n_{\text{train}}} \sum_{i=1}^m \left\| \mathbf{z}^{(\ell)}(t_i) - \tilde{\mathbf{z}}^{(\ell)}(t_i) \right\|_1 + \lambda \|\Xi\|_1, \quad (2)$$

where  $\|X\|_1 = \sum_{l,k} |[X]_{lk}|$ .

**Pruning** Taking linear combinations of candidate functions in Eq. (1) admits implementation as a linear layer, specified by  $\Xi$ , which does not have biases or nonlinear activation. To further sparsify the coefficient matrix  $\Xi$ , we employ the magnitude-based pruning strategy:

$$[\Xi]_{lk} = 0 \quad \text{if} \quad |[\Xi]_{lk}| < \tau \quad (3)$$

We find that pruning is essential to find the sparse representation of  $\Xi$  and will provide empirical evidence obtained from the numerical experiments. In next Section, we detail how we use the pruning strategy during the training process.

## Training

We employ mini-batching to train the proposed neural network architecture. For each training step, we randomly sample  $n_{\text{batch}}$  trajectories from the training set and then randomly sample initial points from the selected  $n_{\text{batch}}$  trajectories to assemble  $n_{\text{batch}}$  sub-sequences of length  $\ell_{\text{batch}}$ . We solve IVPs with the sample initial points, measure the loss (Eq. (2)), and update the model parameters  $\Theta$  via Adamax. After the update, we prune the model parameters using the magnitude-based pruning as shown in (3). Algorithm 1 summarizes the training procedure.

---

### Algorithm 1: Neural SINDy training

---

```

1 Initialize  $\Theta$ 
2 for ( $i = 0$ ;  $i < n_{\text{max}}$ ;  $i = i + 1$ ) do
3   Sample  $n_{\text{batch}}$  trajectories randomly from  $\mathcal{D}_{\text{train}}$ 
4   Sample initial points randomly from the sampled
   trajectories:  $\mathbf{x}_{s(r)}^r, s(r) \in [0, \dots, m - \ell_{\text{batch}} - 1]$ 
   for  $r = 1, \dots, n_{\text{batch}}$ 
5    $\tilde{\mathbf{x}}(t_1), \dots, \tilde{\mathbf{x}}(t_m) = \text{ODESolve}(\mathbf{x}_{s(r)}^r, \mathbf{f}_{\Theta}, t_1, \dots, t_m)$ ,
   for  $r = 1, \dots, n_{\text{batch}}$ 
6   Compute the loss  $\mathcal{L}$  (Eq. (1))
7   Update  $\Theta$  via SGD
8   Prune  $\Theta$  based on the magnitude (Eq. (3))
9 end

```

---

## Experimental results with neural SINDy

We implement the proposed method in PYTHON 3.7.2 and PYTORCH 1.9.0 (Paszke et al. 2019). In all training, we use Adamax (Kingma and Ba 2015) with an initial learning rate 0.01 and use exponential learning rate decay with the multiplicative factor, 0.9987. In the following experiments, we set the penalty weight as  $\lambda = 10^{-4}$  and the pruning threshold as  $\tau = 10^{-6}$ . For ODESolve, we use the Dormand–Prince method (dopri5) (Dormand and Prince 1980) with relative tolerance  $10^{-7}$  and absolute tolerance  $10^{-9}$  unless otherwise specified. All experiments are performed on MACBOOK PRO with M1 CPU and 16 GB memory.

**Dictionary construction** In the following experiment, we employ a set of polynomials,  $\mathcal{P}_{n,d}$ , where  $n$  is the number of variables and  $d$  is the maximal total degree of polynomials in the set. An example set,  $\mathcal{P}_{3,2}$  is given as

$$\mathcal{P}_{3,2} = \{1, x_1, x_1^2, x_1x_2, x_1x_3, x_2, x_2^2, x_2x_3, x_3^2\}.$$

## Experiment set

We examine the performance of the proposed method for a number of dynamical systems (see Table 1 for the equations):

- Hyperbolic example,
- Cubic oscillator,
- Van der Pol oscillator,
- Hopf bifurcation,
- Lorenz system.

To generate data, we base our implementation on the code from (Liu, Kutz, and Brunton 2020): generating 1600 training trajectories, 320 validating trajectories, and 320 test trajectories. For the first four example problems, we use time step size  $\Delta t = 0.01$  and total simulation time  $t \in [0, 51.20]$ . For Lorenz, we use  $\Delta t = 0.0005$  and  $t \in [0, 2.56]$ . For training, we use  $n_{\text{max}} = 500$  and  $n_{\text{max}} = 2000$  for the first four example problems and the last example problem, respectively. In Appendix, a comparison against a “black-box” feed-forward neural network with fully-connected layers is presented; we report the performance of both the black-box neural network and the proposed network measured in terms of time-instantaneous mean-squared error (MSE).

Table 1 shows the ground truth equations and equations identified by using neural SINDy. We use  $\mathcal{P}_{2,3}$ ,  $\mathcal{P}_{3,3}$ , and  $\mathcal{P}_{3,2}$ , respectively, for the first three example problems, the fourth example problem, and the last example problem. During training, coefficients with small magnitude are pruned (i.e., setting them as 0) and are not presented in Table. We also report the learned coefficients without the pruning strategy in Appendix, which highlights that the pruning is required to zero out the coefficients of small magnitude.

Figure 1 depicts examples of reference trajectories and trajectories computed from identified dynamics, where the trajectories are chosen from the test set. As reported in the Appendix, time-instantaneous MSEs computed by nSINDy are several orders of magnitude smaller ( $10^6 \sim 10^8$  smaller) than those computed by the black-box NODEs.

## Neural SINDy for structure preserving parameterization

### GENERIC structure-preserving parameterization

In the following, we present neural SINDy for a structure-preserving reversible and irreversible dynamics modeling approach. An alternative formalism for irreversible dynamics based on port-Hamiltonians is included in the appendix.

**GENERIC formalism** We begin by reviewing the general equation for the nonequilibrium reversible–irreversible coupling (GENERIC) formalism.

In GENERIC, the evolution of an observable  $A(\mathbf{x})$  is assumed to evolve under the gradient flow

$$\frac{dA}{dt} = \{A, E\} + [A, S]$$

where  $E$  and  $S$  denote generalized energy and entropy, and  $\{\cdot, \cdot\}$  and  $[\cdot, \cdot]$  denote a Poisson bracket and an irreversible metric bracket. The Poisson bracket is given in terms of a skew-symmetric Poisson matrix  $L$  and the irreversible bracket is given in terms of a symmetric positive semi-definite friction matrix  $M$ ,

$$\{A, B\} = \frac{\partial A}{\partial \mathbf{x}} L \frac{\partial B}{\partial \mathbf{x}}, \quad \text{and} \quad [A, B] = \frac{\partial A}{\partial \mathbf{x}} M \frac{\partial B}{\partial \mathbf{x}}.$$

Lastly, the GENERIC formalism requires two degeneracy conditions defined as

$$L \frac{\partial S}{\partial \mathbf{x}} = 0, \quad \text{and} \quad M \frac{\partial E}{\partial \mathbf{x}} = 0.$$

Eq. name	Ground truth	Identified
Hyperbolic	$\dot{x} = -0.05x$ $\dot{y} = x^2 - y$	$\dot{x} = -0.050006x$ $\dot{y} = 1.000063x^2 - 1.000063y$
Cubic oscillator	$\dot{x} = -0.1x^3 + 2y^3$ $\dot{y} = -2x^3 - 0.1y^3$	$\dot{x} = -0.100075x^3 + 2.000019y^3$ $\dot{y} = -1.999906x^3 - 0.099915y^3$
Van der Pol	$\dot{x} = y$ $\dot{y} = -x + 2y - 2x^2y$	$\dot{x} = 1.000015y$ $\dot{y} = -1.000043x + 2.000271y - 1.999807x^2y$
Hopf bifurcation	$\dot{\mu} = 0$ $\dot{x} = \mu x + y - x^3 - xy^2$ $\dot{y} = \mu y - x - yx^2 - y^3$	$\dot{\mu} = 0$ $\dot{x} = 0.999237\mu x + 1.000174y - 0.999523x^3 - 0.999582xy^2$ $\dot{y} = 0.999515\mu y - 0.999821x - 0.999276yx^2 - 0.999409y^3$
Lorenz	$\dot{x} = -10x + 10y$ $\dot{y} = 28x - xz - y$ $\dot{z} = xy - \frac{8}{3}z$	$\dot{x} = -10.000108x + 9.999878y$ $\dot{y} = 27.999895x - 0.999998xz - 0.999883y$ $\dot{z} = 1.000017xy - 2.666697z$

Table 1: [nSINDy experiments] The equation names, the ground truth equations, and the identified equations by using nSINDy.

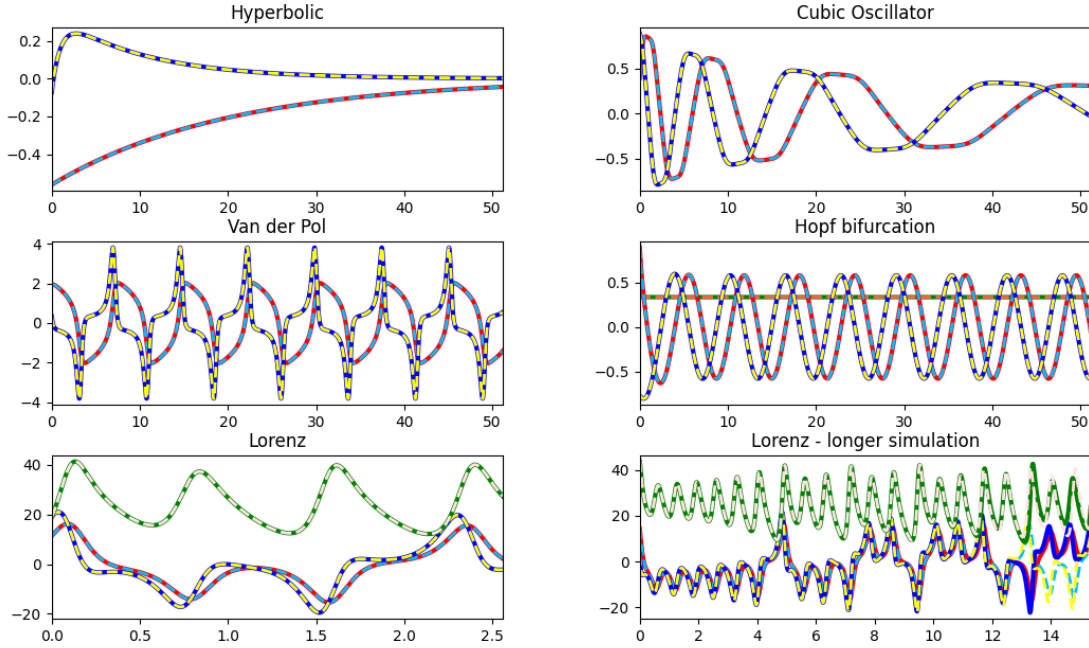


Figure 1: [nSINDy experiments] Examples of reference trajectories (solid lines) and computed trajectories (dashed lines) from learned dynamics.

With the state variables  $\mathbf{x} = [q, p, S]^\top$ , the GENERIC formalism defines the evolution of  $\mathbf{x}$  as

$$\frac{d\mathbf{x}}{dt} = L \frac{\partial E}{\partial \mathbf{x}} + M \frac{\partial S}{\partial \mathbf{x}}. \quad (4)$$

**Parameterization for GENERIC** Here, we review the parameterization technique, developed in (Oettinger 2014) and further extended into deep learning settings in (Lee, Trask, and Stinis 2021). As for the Hamiltonian Eq. (5), we parameterize the total energy such as

$$E_{\theta_1}(q, p, S) = (\phi(q, p, S)^\top \Xi)^\top,$$

with  $\theta_1 = \Xi$ . Then we parameterize the symmetric irreversible dynamics via the bracket

$$[A, B]_{\theta_2} = \zeta_{\alpha\beta, \mu\nu} \frac{\partial A}{\partial x_\alpha} \frac{\partial E_{\theta_1}}{\partial x_\beta} \frac{\partial B}{\partial x_\mu} \frac{\partial E_{\theta_1}}{\partial x_\nu},$$

where

$$\zeta_{\alpha\beta, \mu\nu} = \Lambda_{\alpha\beta}^m D_{mn} \Lambda_{\mu\nu}^n.$$

The matrices,  $\Lambda$  and  $D$ , are skew-symmetric and symmetric positive semi-definite matrices, respectively, such that

$$\Lambda_{\alpha\beta}^m = -\Lambda_{\beta\alpha}^m, \quad \text{and} \quad D_{mn} = D_{nm},$$

where the skew-symmetry and the symmetric positive semi-definiteness can be achieved by the parameterization tricks

$$\Lambda = \frac{1}{2}(\tilde{\Lambda} - \tilde{\Lambda}^\top), \quad \text{and} \quad D = \tilde{D}\tilde{D}^\top,$$

where  $\tilde{\Lambda}$  and  $\tilde{D}$  are matrices with learnable entries and, thus,  $\theta_2 = [\tilde{\Lambda}, \tilde{D}]$ .

With this parameterization, the irreversible part of the dynamics is given by

$$[\mathbf{x}, S]_{\theta_2} = M_{\theta_2} \frac{\partial S}{\partial \mathbf{x}} = \zeta_{\alpha\beta, \mu\nu} \frac{\partial E_{\theta_1}}{\partial x_\beta} \frac{\partial S}{\partial x_\mu} \frac{\partial E_{\theta_1}}{\partial x_\nu}$$

Eq. name	Parameterization	Ground truth	Identified
DNO	nSINDy	$\dot{q} = p$ $\dot{p} = -3 \sin(q) - 0.04p$ $\dot{S} = 0.04p^2$	$\dot{q} = 0.999622p$ $\dot{p} = -2.8645 \sin(q) - 0.04001p - 0.1340q + 0.0190q^3$ $\dot{S} = 0.040081p^2$
	nSINDy - GNN	$E = 0.5p^2 - 3 \cos(q) + S$	$E_{\theta_1} = 0.500144p^2 - 2.999785 \cos(q) + 0.998337S$

Table 2: [GENERIC structure preservation] The equation names, the ground truth equations, and the identified equations by using nSINDy (non structure preserving parameterization) and nSINDy - GNN (GENERIC structure preserving parameterization).

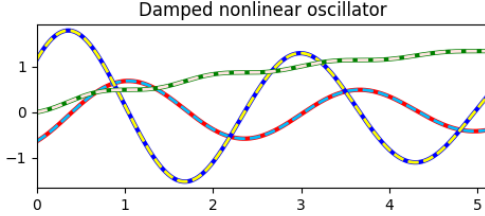


Figure 2: [GENERIC structure preservation] Examples of reference trajectories (solid lines) and computed trajectories (dashed lines) from learned dynamics.

and, as a result,  $f_{\Theta}$  is now defined as

$$f_{\Theta} = \{\mathbf{x}, E_{\theta_1}\} + [\mathbf{x}, S] = L \frac{\partial E_{\theta_1}}{\partial \mathbf{x}} + M_{\theta_2} \frac{\partial S}{\partial \mathbf{x}},$$

with  $\Theta = [\theta_1, \theta_2]$ .

**Experiments** An example problem (with their reference mathematical formulations) considered in this paper is:

- Damped nonlinear oscillator from (Shang and Öttinger 2020): the ground truth equation can be written in the GENERIC formalism (Eq. (4)) with the following components:

$$L = \begin{bmatrix} 0 & 1 & 0 \\ -1 & 0 & 0 \\ 0 & 0 & 0 \end{bmatrix}, \quad M = 0.04 \begin{bmatrix} 0 & 0 & 0 \\ 0 & 1 & -p \\ 0 & -p & p^2 \end{bmatrix},$$

$$\text{and } E(q, p, S) = \frac{p^2}{2} - 3 \cos(q) + S.$$

Alternatively, the equation for the dynamics can be written as

$$\begin{aligned} \dot{q} &= p, \\ \dot{p} &= -3 \sin(q) - 0.04p \\ \dot{S} &= 0.04p^2. \end{aligned}$$

In the experiment, we assume that we have knowledge on  $L$  and that the measurements on  $S$  are available. That is, the nSINDy method with the GENERIC structure preservation seeks the unknown  $M$  and  $E$ . For generating data, we base our implementation on the code from (Shang and Öttinger 2020). We generate 800 training trajectories, 160 validation trajectories, and 160 test trajectories with  $\Delta t = 0.001$  and the simulation time  $[0, 5.12]$ . We use a dictionary consisting of polynomials and trigonometric functions:

$$\mathcal{P} = \{\mathcal{P}_{2,3}, \cos(q), \sin(q), \cos(p), \sin(p)\}.$$

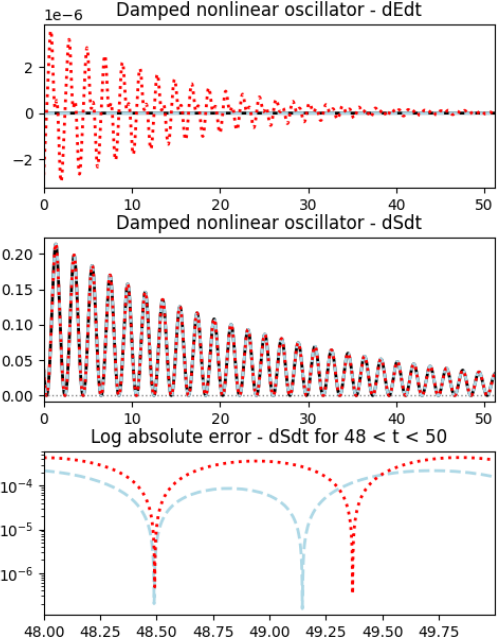


Figure 3: [GENERIC structure preservation]  $\frac{dE}{dt}$  and  $\frac{dS}{dt}$  of the reference system (black solid line), the system identified by nSINDy (red dotted line), and the system identified by nSINDy - GNN (lightblue dashed line).

We consider the same experimental settings that are used in the above experiments: Adamax optimizer with the initial learning rate 0.01, exponential learning rate decay with a factor 0.9987, L1-penalty weight  $10^{-4}$ , pruning threshold  $10^{-6}$ , dopri5 for the ODE integrator with  $10^{-7}$  and  $10^{-9}$  for relative and absolute tolerances, and, finally,  $n_{\max} = 300$ .

Table 2 reports the coefficients of the identified systems when nSINDy and nSINDy - GNN are used. With  $n_{\max} = 300$ , nSINDy fails to correctly identify the system, whereas nSINDy - GNN identifies the exact terms correctly and computes the coefficients accurately. Figure 2 depicts the ground truth trajectory and the trajectory computed from the learned dynamics function (nSINDy - GNN). Figure 3 shows the advantages of using GENERIC structure preservation via plots of  $\frac{dE}{dt}$  and  $\frac{dS}{dt}$ . The difference between structure-preserving and non-structure-preserving parameterization is shown dramatically in the plot of  $\frac{dE}{dt}$ ; the structure-preserving parameterization produces  $\frac{dE}{dt} = 0$ , whereas the non-structure-preserving parameterization produces fluctuating values of

Eq. name	Parameterization	Ground truth	Identified
Ideal mass-spring	nSINDy	$\dot{q} = p$ $\dot{p} = -q$	$\dot{q} = 0.999989p$ $\dot{p} = -1.000030q$
	nSINDy - HNN	$\mathcal{H}(q, p) = 0.5q^2 + 0.5p^2$	$\mathcal{H}(q, p) = 0.499991q^2 + 0.500033p^2$
Ideal pendulum	nSINDy	$\dot{q} = p$ $\dot{p} = -6 \sin(q)$	$\dot{q} = 1.000018p + 0.034095q - 0.004796q^3$ $\dot{p} = -5.890695 \sin(q) - 0.107052q$
	nSINDy - HNN	$\mathcal{H}(q, p) = 6 - 6 \cos(q) + 0.5p^2$	$\mathcal{H}(q, p) = 6 - 5.999838 \cos(q) + 0.500014p^2$

Table 3: [Hamiltonian structure preservation] The equation names, the ground truth equations, and the identified equations by using nSINDy (non structure preserving parameterization) and nSINDy - HNN (Hamiltonian structure preserving parameterization).

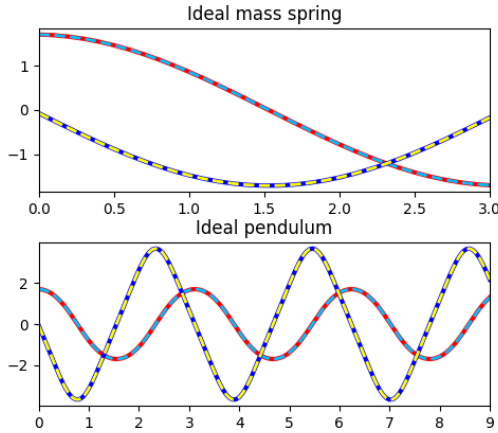


Figure 4: [Hamiltonian structure preservation] Examples of reference trajectories (solid lines) and computed trajectories (dashed lines) from learned dynamics.

$$\frac{dE}{dt}.$$

### Hamiltonian structure-preserving parameterization

In the following, we consider the Hamiltonian structure-preserving parameterization technique proposed in Hamiltonian neural networks (HNNs) (Greydanus, Dzamba, and Yosinski 2019): parameterizing the Hamiltonian function  $\mathcal{H}(q, p)$  as  $\mathcal{H}_\Theta(q, p)$  such that

$$\mathcal{H}_\Theta = (\phi(q, p)^\top \Xi)^\top. \quad (5)$$

With the above parameterization and  $\mathbf{x} = [q, p]^\top$ , the dynamics can be modeled as

$$\begin{bmatrix} \frac{dq}{dt} \\ \frac{dp}{dt} \end{bmatrix} = \begin{bmatrix} -\frac{\partial \mathcal{H}_\Theta}{\partial p} \\ \frac{\partial \mathcal{H}_\Theta}{\partial q} \end{bmatrix},$$

i.e.,  $\mathbf{f}_\Theta$  is now defined as  $\mathbf{f}_\Theta = [-\frac{\partial \mathcal{H}_\Theta}{\partial p}, \frac{\partial \mathcal{H}_\Theta}{\partial q}]^\top$ . Then the loss objective can be written as

$$\left\| \frac{\partial \mathcal{H}_\Theta}{\partial p} - \frac{dq}{dt} \right\|_1 + \left\| \frac{\partial \mathcal{H}_\Theta}{\partial q} + \frac{dp}{dt} \right\|_1.$$

As noted in (Lee, Trask, and Stinis 2021), with canonical coordinates  $\mathbf{x} = [q, p]^\top$ , and canonical Poisson matrix  $L =$

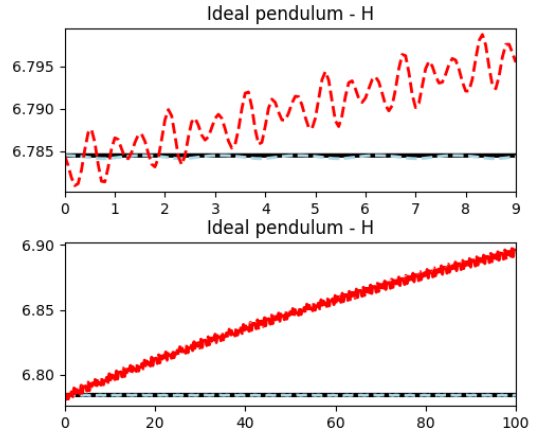


Figure 5: [Hamiltonian structure preservation] The Hamiltonian function measured by the trajectories computed with nSINDy (red dashed line) and nSINDy-HNN (blue dashed line). Figure below depicts the Hamiltonian functions measured by the trajectories computed for extended numerical simulation time, i.e., 100 seconds (the training simulation time is 9 seconds).

$\begin{bmatrix} 0 & 1 \\ -1 & 0 \end{bmatrix}$ , and  $M = \mathbf{0}$ , the GENERIC formalism in Eq. (4) recovers Hamiltonian dynamics.

**Experiments** We examine the performance of the proposed method with a list of example dynamic systems:

- Ideal mass-spring,
- Ideal pendulum.

For generating data, we base our implementation on the code from (Greydanus, Dzamba, and Yosinski 2019). We generate 800 training trajectories, 160 validation trajectories, and 160 test trajectories. For the mass spring and the pendulum problem, we use  $\Delta t = 0.1$  and  $\Delta t = 1/15$ , respectively, and the simulation time is set as  $[0, 3]$  and  $[0, 9]$ , respectively.

Table 3 shows the ground truth equations and equations identified by using neural SINDy. For the mass spring problem, we use  $\mathcal{P}_{2,3}$  and for the pendulum problem we use a dictionary consisting of polynomials and trigonometric functions:

$$\mathcal{P} = \{\mathcal{P}_{2,3}, \cos(q), \sin(q), \cos(p), \sin(p)\}.$$

Again, we use the same experimental settings described above for the GENERIC parameterization. In Table 3, we presented results obtained by two different parameterization techniques: 1) the “plain” dictionary approach (Eq. (1)) denoted by (nSINDy) and 2) the Hamiltonian approach (Eq (5)) denoted by (nSINDy - HNN).

Figure 4 depicts examples of reference trajectories and trajectories computed from identified dynamics, where the trajectories are chosen from the test set. Figure 5 depicts how the energy is being conserved in the dynamics learned with nSINDy-HNN, whereas the plain approach (nSINDy) fails to conserve the energy.

## Discussion

**Limitation** The proposed method shares the same limitations of the original SINDy method: successful identification requires inclusion of the correct dictionaries in the library. Potential alternatives are well-studied in the literature and include either adding an extra “black-box” neural network to compensate missing dictionaries or designing a neural network that can learn dictionaries from data (such as in (Sahoo, Lampert, and Martius 2018)).

The gradient-based parameter update and the magnitude-based pruning could potentially zero out unwanted coefficients in a special case: when the signs of the coefficients need to be changed in the later stage of the training. If the magnitude of the loss term becomes very small (and the gradient as well), the updated coefficients may satisfy the pruning condition shown in (3).

Lastly, when adaptive step-size ODE solvers are used (e.g., dopri5), numerical underflow may occur. This can be mitigated by trying different initialization for the coefficients, or smaller batch length  $\ell_{\text{batch}}$ . However, further study regarding robust initialization is required.

## Related work

**System identification** In (Schmidt and Lipson 2009), the proposed method uses a genetic algorithms to identify governing physical laws (Lagrangian or Hamiltonian) from measurements of real experiments. A seminal work on sparse regression methods for system identification has been proposed in (Brunton, Proctor, and Kutz 2016). Then the sparse regression methods have been extended to various settings, e.g., for model predictive control (Kaiser, Kutz, and Brunton 2018), and for identifying dynamics in latent space using autoencoders (Hinton and Salakhutdinov 2006) and then learning parsimonious representations for the latent dynamics (Champion et al. 2019). Also, the sparse regression methods have been applied for identifying partial differential equations (PDEs) (Rudy et al. 2017, 2019). For identifying PDEs, deep-learning-based approaches such as physics-informed neural networks (Raissi, Perdikaris, and Karniadakis 2019) and PDE-net (Long et al. 2018) have been studied recently.

**Structure preserving neural network** Designing neural network architectures that exactly enforces important physical properties has been an important topic and studied extensively. Parameterization techniques that preserve physical

structure include Hamiltonian neural networks (Greydanus, Dzamba, and Yosinski 2019; Toth et al. 2019), Lagrangian neural networks (Cranmer et al. 2020; Lutter, Ritter, and Peters 2018), port-Hamiltonian neural networks (Desai et al. 2021), and GENERIC neural networks (Hernández et al. 2021; Lee, Trask, and Stinis 2021). Neural network architectures that mimic the action of symplectic integrators have been proposed in (Chen et al. 2019; Jin et al. 2020; Tong et al. 2021), and a training algorithm exploiting physical invariance for learning dynamical systems, e.g., time-reversal symmetric, has been studied in (Huh et al. 2020).

## Conclusion

We have proposed a simple and effective deep-learning-based training algorithm for a dictionary-based parameterization of nonlinear dynamics. The proposed algorithm is based on the training procedure introduced in neural ordinary differential equations (NODE) (Chen et al. 2018) and employs L1-weight decay of model parameters and magnitude-based pruning strategy, inspired by sparse identification of nonlinear dynamics (SINDy) (Brunton, Proctor, and Kutz 2016). We have further extended the dictionary-based parameterization approach to structure-preserving parameterization techniques, such as Hamiltonian neural networks, GENERIC neural networks, and port-Hamiltonian networks. For a suite of benchmark problems, we have demonstrated that the proposed training algorithm is very effective in identifying the underlying dynamics from data with expected gains from imposing structure-preservation.

## Acknowledgments

N. Trask and P. Stinis acknowledge funding under the Collaboratory on Mathematics and Physics-Informed Learning Machines for Multiscale and Multiphysics Problems (PhILMs) project funded by DOE Office of Science (Grant number DE-SC001924). N. Trask and K. Lee acknowledge funding from the DOE Early Career program. Sandia National Laboratories is a multi-mission laboratory managed and operated by National Technology and Engineering Solutions of Sandia, LLC., a wholly owned subsidiary of Honeywell International, Inc., for the U.S. Department of Energy’s National Nuclear Security Administration under contract DE-NA0003525. This paper describes objective technical results and analysis. Any subjective views or opinions that might be expressed in the paper do not necessarily represent the views of the U.S. Department of Energy or the United States Government.

## References

- Alexopoulos, K.; Nikolakis, N.; and Chryssoulouris, G. 2020. Digital twin-driven supervised machine learning for the development of artificial intelligence applications in manufacturing. *International Journal of Computer Integrated Manufacturing*, 33(5): 429–439.
- Baker, N.; Alexander, F.; Bremer, T.; Hagberg, A.; Kevrekidis, Y.; Najm, H.; Parashar, M.; Patra, A.; Sethian, J.; Wild, S.; et al. 2019. Workshop report on basic research needs for scientific machine learning: Core technologies for

- artificial intelligence. Technical report, USDOE Office of Science (SC), Washington, DC (United States).
- Bertalan, T.; Dietrich, F.; Mezić, I.; and Kevrekidis, I. G. 2019. On learning Hamiltonian systems from data. *Chaos: An Interdisciplinary Journal of Nonlinear Science*, 29(12): 121107.
- Brunton, S. L.; Proctor, J. L.; and Kutz, J. N. 2016. Discovering governing equations from data by sparse identification of nonlinear dynamical systems. *Proceedings of the National Academy of Sciences*, 113(15): 3932–3937.
- Champion, K.; Lusch, B.; Kutz, J. N.; and Brunton, S. L. 2019. Data-driven discovery of coordinates and governing equations. *Proceedings of the National Academy of Sciences*, 116(45): 22445–22451.
- Chen, R.; and Tao, M. 2021. Data-driven Prediction of General Hamiltonian Dynamics via Learning Exactly-Symplectic Maps. *arXiv preprint arXiv:2103.05632*.
- Chen, R. T.; Rubanova, Y.; Bettencourt, J.; and Duvenaud, D. 2018. Neural ordinary differential equations. In *Proceedings of the 32nd International Conference on Neural Information Processing Systems*, 6572–6583.
- Chen, W.; Wang, Q.; Hesthaven, J. S.; and Zhang, C. 2021. Physics-informed machine learning for reduced-order modeling of nonlinear problems. *Journal of Computational Physics*, 110666.
- Chen, Z.; Zhang, J.; Arjovsky, M.; and Bottou, L. 2019. Symplectic Recurrent Neural Networks. In *International Conference on Learning Representations*.
- Cranmer, M.; Greydanus, S.; Hoyer, S.; Battaglia, P.; Spergel, D.; and Ho, S. 2020. Lagrangian Neural Networks. In *ICLR 2020 Workshop on Integration of Deep Neural Models and Differential Equations*.
- Desai, S.; Mattheakis, M.; Sondak, D.; Protopapas, P.; and Roberts, S. 2021. Port-Hamiltonian Neural Networks for Learning Explicit Time-Dependent Dynamical Systems. *arXiv preprint arXiv:2107.08024*.
- Dormand, J. R.; and Prince, P. J. 1980. A family of embedded Runge-Kutta formulae. *Journal of computational and applied mathematics*, 6(1): 19–26.
- Ghnatios, C.; Alfaro, I.; González, D.; Chinesta, F.; and Cueto, E. 2019. Data-driven generic modeling of poroviscoelastic materials. *Entropy*, 21(12): 1165.
- Greydanus, S.; Dzamba, M.; and Yosinski, J. 2019. Hamiltonian Neural Networks. In Wallach, H. M.; Larochelle, H.; Beygelzimer, A.; d’Alché-Buc, F.; Fox, E. B.; and Garnett, R., eds., *Advances in Neural Information Processing Systems 32*, 15353–15363.
- Hairer, E.; Hochbruck, M.; Iserles, A.; and Lubich, C. 2006. Geometric numerical integration. *Oberwolfach Reports*, 3(1): 805–882.
- Hernández, Q.; Badías, A.; González, D.; Chinesta, F.; and Cueto, E. 2021. Structure-preserving neural networks. *Journal of Computational Physics*, 426: 109950.
- Hinton, G. E.; and Salakhutdinov, R. R. 2006. Reducing the dimensionality of data with neural networks. *science*, 313(5786): 504–507.
- Huh, I.; Yang, E.; Hwang, S. J.; and Shin, J. 2020. Time-Reversal Symmetric ODE Network. *Advances in Neural Information Processing Systems*, 33.
- Jin, P.; Zhang, Z.; Zhu, A.; Tang, Y.; and Karniadakis, G. E. 2020. SympNets: Intrinsic structure-preserving symplectic networks for identifying Hamiltonian systems. *Neural Networks*, 132: 166–179.
- Kaiser, E.; Kutz, J. N.; and Brunton, S. L. 2018. Sparse identification of nonlinear dynamics for model predictive control in the low-data limit. *Proceedings of the Royal Society A*, 474(2219): 20180335.
- Karapiperis, K.; Stainier, L.; Ortiz, M.; and Andrade, J. 2021. Data-driven multiscale modeling in mechanics. *Journal of the Mechanics and Physics of Solids*, 147: 104239.
- Karniadakis, G. E.; Kevrekidis, I. G.; Lu, L.; Perdikaris, P.; Wang, S.; and Yang, L. 2021. Physics-informed machine learning. *Nature Reviews Physics*, 3(6): 422–440.
- Kingma, D. P.; and Ba, J. 2015. Adam: A Method for Stochastic Optimization. In *3rd International Conference on Learning Representations, ICLR*.
- Lee, K.; and Carlberg, K. T. 2021. Deep Conservation: A Latent-Dynamics Model for Exact Satisfaction of Physical Conservation Laws. In *Proceedings of the AAAI Conference on Artificial Intelligence*, volume 35, 277–285.
- Lee, K.; Trask, N. A.; and Stinis, P. 2021. Machine learning structure preserving brackets for forecasting irreversible processes. *arXiv preprint arXiv:2106.12619*.
- Liu, Y.; Kutz, J. N.; and Brunton, S. L. 2020. Hierarchical deep learning of multiscale differential equation time-steppers. *arXiv preprint arXiv:2008.09768*.
- Long, Z.; Lu, Y.; Ma, X.; and Dong, B. 2018. Pde-net: Learning pdes from data. In *International Conference on Machine Learning*, 3208–3216. PMLR.
- Lutter, M.; Ritter, C.; and Peters, J. 2018. Deep Lagrangian Networks: Using Physics as Model Prior for Deep Learning. In *International Conference on Learning Representations*.
- Marsden, J. E.; and Ratiu, T. S. 1995. Introduction to mechanics and symmetry. *Physics Today*, 48(12): 65.
- Masi, F.; Stefanou, I.; Vannucci, P.; and Maffi-Berthier, V. 2021. Thermodynamics-based Artificial Neural Networks for constitutive modeling. *Journal of the Mechanics and Physics of Solids*, 147: 104277.
- Oettinger, H. C. 2014. Irreversible dynamics, Onsager-Casimir symmetry, and an application to turbulence. *Physical Review E*, 90(4): 042121.
- Paszke, A.; Gross, S.; Massa, F.; Lerer, A.; Bradbury, J.; Chanan, G.; Killeen, T.; Lin, Z.; Gimelshein, N.; Antiga, L.; Desmaison, A.; Köpf, A.; Yang, E.; DeVito, Z.; Raison, M.; Tejani, A.; Chilamkurthy, S.; Steiner, B.; Fang, L.; Bai, J.; and Chintala, S. 2019. PyTorch: An Imperative Style, High-Performance Deep Learning Library. In *Advances in Neural Information Processing Systems 32*, 8024–8035.
- Patel, R. G.; Manickam, I.; Trask, N. A.; Wood, M. A.; Lee, M.; Tomas, I.; and Cyr, E. C. 2020. Thermodynamically consistent physics-informed neural networks for hyperbolic systems. *arXiv preprint arXiv:2012.05343*.

- Raissi, M.; Perdikaris, P.; and Karniadakis, G. E. 2019. Physics-informed neural networks: A deep learning framework for solving forward and inverse problems involving nonlinear partial differential equations. *Journal of Computational Physics*, 378: 686–707.
- Rohrhofer, F. M.; Posch, S.; and Geiger, B. C. 2021. On the Pareto Front of Physics-Informed Neural Networks. *arXiv preprint arXiv:2105.00862*.
- Rudy, S.; Alla, A.; Brunton, S. L.; and Kutz, J. N. 2019. Data-driven identification of parametric partial differential equations. *SIAM Journal on Applied Dynamical Systems*, 18(2): 643–660.
- Rudy, S. H.; Brunton, S. L.; Proctor, J. L.; and Kutz, J. N. 2017. Data-driven discovery of partial differential equations. *Science Advances*, 3(4): e1602614.
- Sahoo, S.; Lampert, C.; and Martius, G. 2018. Learning equations for extrapolation and control. In *International Conference on Machine Learning*, 4442–4450. PMLR.
- Schmidt, M.; and Lipson, H. 2009. Distilling free-form natural laws from experimental data. *science*, 324(5923): 81–85.
- Shang, X.; and Öttinger, H. C. 2020. Structure-preserving integrators for dissipative systems based on reversible–irreversible splitting. *Proceedings of the Royal Society A*, 476(2234): 20190446.
- Tibshirani, R. 1996. Regression shrinkage and selection via the Lasso. *Journal of the Royal Statistical Society: Series B (Methodological)*, 58(1): 267–288.
- Tong, Y.; Xiong, S.; He, X.; Pan, G.; and Zhu, B. 2021. Symplectic neural networks in Taylor series form for Hamiltonian systems. *Journal of Computational Physics*, 110325.
- Toth, P.; Rezende, D. J.; Jaegle, A.; Racanière, S.; Botev, A.; and Higgins, I. 2019. Hamiltonian Generative Networks. In *International Conference on Learning Representations*.
- Trask, N.; Huang, A.; and Hu, X. 2020. Enforcing exact physics in scientific machine learning: a data-driven exterior calculus on graphs. *arXiv preprint arXiv:2012.11799*.
- Wan, Z. Y.; Vlachas, P.; Koumoutsakos, P.; and Sapsis, T. 2018. Data-assisted reduced-order modeling of extreme events in complex dynamical systems. *PloS one*, 13(5): e0197704.
- Wang, S.; Teng, Y.; and Perdikaris, P. 2020. Understanding and mitigating gradient pathologies in physics-informed neural networks. *arXiv preprint arXiv:2001.04536*.
- Wu, J.-L.; Xiao, H.; and Paterson, E. 2018. Physics-informed machine learning approach for augmenting turbulence models: A comprehensive framework. *Physical Review Fluids*, 3(7): 074602.
- Yu, H.; Tian, X.; Li, Q.; et al. 2020. OnsagerNet: Learning Stable and Interpretable Dynamics using a Generalized Onsager Principle. *arXiv preprint arXiv:2009.02327*.
- Zhong, Y. D.; Dey, B.; and Chakraborty, A. 2020. Dissipative symoden: Encoding Hamiltonian dynamics with dissipation and control into deep learning. *arXiv preprint arXiv:2002.08860*.
- Zhong, Y. D.; Dey, B.; and Chakraborty, A. 2021. Benchmarking Energy-Conserving Neural Networks for Learning Dynamics from Data. In *Learning for Dynamics and Control*, 1218–1229. PMLR.

## Training without pruning

Tables 4 and 5 report the coefficients learned by training without the pruning-strategy. Although the algorithm successfully finds the significant coefficients, it fails to zero out the coefficients of the small contributions.

	Hyperbolic		Cubic oscillator		Van der Pol	
	$\dot{x} = -0.05x$ $\dot{y} = 1x^2 - 1y$		$\dot{x} = -0.1x^3 + 2y^3$ $\dot{y} = -2x^3 - 0.1y^3$		$\dot{x} = 1y$ $\dot{y} = -1x + 2y - 2x^2y$	
	$\dot{x}$	$\dot{y}$	$\dot{x}$	$\dot{y}$	$\dot{x}$	$\dot{y}$
1	-4.0265e-04	-1.5801e-04	-1.1837e-04	-1.9252e-04	7.6617e-04	-4.6053e-04
$x$	<b>-4.8321e-02</b>	6.7640e-04	-3.8775e-04	2.1818e-05	-4.3242e-04	<b>-9.9930e-01</b>
$y$	2.2759e-05	<b>-9.9818e-01</b>	3.4231e-04	5.1497e-04	<b>1.0002e+00</b>	<b>1.9997e+00</b>
$x^2$	1.1598e-04	<b>1.0021e+00</b>	8.5114e-04	-1.0675e-04	-4.3595e-06	-2.6983e-04
$xy$	-9.0811e-04	1.3638e-03	3.9183e-04	-1.0255e-04	1.3413e-03	1.3681e-04
$y^2$	-9.9513e-04	1.2584e-03	4.7589e-04	-3.6600e-04	8.9859e-04	-5.9787e-04
$x^3$	2.3237e-03	-1.3569e-03	<b>-9.9985e-02</b>	<b>-2.0003e+00</b>	6.0941e-05	-5.1159e-05
$x^2y$	-7.3889e-04	1.1560e-03	-8.8203e-04	8.3778e-04	1.6378e-04	<b>-2.0006e+00</b>
$xy^2$	-3.7055e-04	3.2972e-04	-3.6603e-04	-6.3260e-04	3.8560e-04	3.5658e-04
$y^3$	-2.8758e-03	3.6145e-04	<b>2.0003e+00</b>	<b>-1.0056e-01</b>	1.3837e-04	6.8370e-05

Table 4: [Hyperbolic, cubic oscillator, and Van der Pol problems] The coefficients learned by nSINDy via training without the magnitude-based pruning strategy.

	Hopf bifurcation			Lorenz		
	$\dot{x} = 1x\mu + 1y - 1x^3 - 1xy^2$ $\dot{y} = 1y\mu - 1x - 1x^2y - 1y^3$ $\dot{\mu} = 0$			$\dot{x} = -10x + 10y$ $\dot{y} = 28x - 1xz - 1y$ $\dot{z} = 1xy - 8/3z$		
	$\dot{x}$	$\dot{y}$	$\dot{\mu}$	$\dot{x}$	$\dot{y}$	$\dot{z}$
1	-7.7859e-05	-5.4043e-05	<b>7.5873e-05</b>	1	5.1030e-07	-5.2767e-07
$x$	-9.0900e-05	<b>-1.0005e+00</b>	-2.7873e-04	$x$	<b>5.6920e-01</b>	<b>1.1720e+01</b>
$y$	<b>9.9948e-01</b>	-1.6792e-04	-3.3130e-04	$y$	<b>4.5274e+00</b>	<b>7.2215e+00</b>
$\mu$	-2.5933e-04	5.7727e-04	4.2798e-04	$z$	5.4791e-07	-3.4551e-06
$x^2$	-3.8502e-04	7.2785e-04	-2.8368e-04	$x^2$	-1.7573e-06	1.7074e-06
$xy$	1.6046e-03	-4.7278e-05	1.6167e-03	$xy$	-1.4202e-06	1.6468e-06
$x\mu$	<b>9.9672e-01</b>	-3.5927e-04	-5.1250e-04	$xz$	-9.4857e-01	<b>4.6996e-01</b>
$y^2$	3.8864e-04	3.1930e-04	-2.0894e-04	$y^2$	-1.5292e-06	8.3760e-06
$y\mu$	-4.5870e-04	<b>9.9483e-01</b>	-8.0084e-04	$yz$	4.5105e-01	-6.7203e-01
$\mu^2$	2.6971e-04	5.6016e-04	2.3888e-04	$z^2$	-8.3810e-05	1.1768e-04
$x^3$	<b>-9.9727e-01</b>	1.3899e-05	-1.2669e-03	$x^3$	-5.9848e-02	9.4702e-02
$x^2y$	-2.1682e-03	<b>-9.9460e-01</b>	-5.3697e-04	$x^2y$	6.0315e-02	-8.9793e-02
$x^2\mu$	-2.4824e-04	5.5955e-04	-2.7237e-04	$x^2z$	-5.6009e-06	5.7127e-06
$xy^2$	<b>-9.9607e-01</b>	-1.2029e-03	-4.7030e-04	$xy^2$	-1.9930e-02	2.6786e-02
$xy\mu$	5.4106e-04	8.6669e-04	-8.0186e-04	$xyz$	1.1614e-05	-1.3253e-05
$x\mu^2$	-9.1186e-04	1.8879e-06	-1.3931e-04	$xz^2$	2.1789e-02	-3.3973e-02
$y^3$	7.2948e-05	<b>-9.9499e-01</b>	-1.5385e-04	$y^3$	2.8419e-03	-3.5977e-03
$y^2\mu$	3.1669e-04	-2.1393e-04	1.0944e-03	$y^2z$	4.1031e-07	-4.9989e-07
$y\mu^2$	-4.0919e-04	-5.7416e-04	7.1154e-04	$yz^2$	-8.8740e-03	1.2924e-02
$\mu^3$	3.7226e-04	1.8204e-04	9.8719e-05	$z^3$	2.7687e-06	-3.6289e-06

Table 5: [Hopf bifurcation and Lorenz] The coefficients learned by nSINDy via training without the magnitude-based pruning strategy.

## Comparison with MLP

Figure depict time-instantaneous mean-squared errors measured between the ground truth trajectories and the trajectories computed from the learned dynamics functions,  $f_{\theta}$ . We consider the two models: the black-box neural ODE models and the proposed SINDy models. For the SINDy models, we use the same experimental settings considered in Experimental results Section. For the black-box neural ODE models, we consider feed-forward neural networks consisting of four layers with 100 neurons in each layer with the hyperbolic Tangent nonlinear activation (Tanh). For training the both models, we use the same optimizer, Adamax, and use the same initial learning rate 0.01 with the same decay strategy (i.e., exponential decay with the multiplicative factor 0.9987). Both models are trained over 500 epochs and 2000 epochs, respectively, for the first four benchmark problems and the last benchmark problem, respectively.

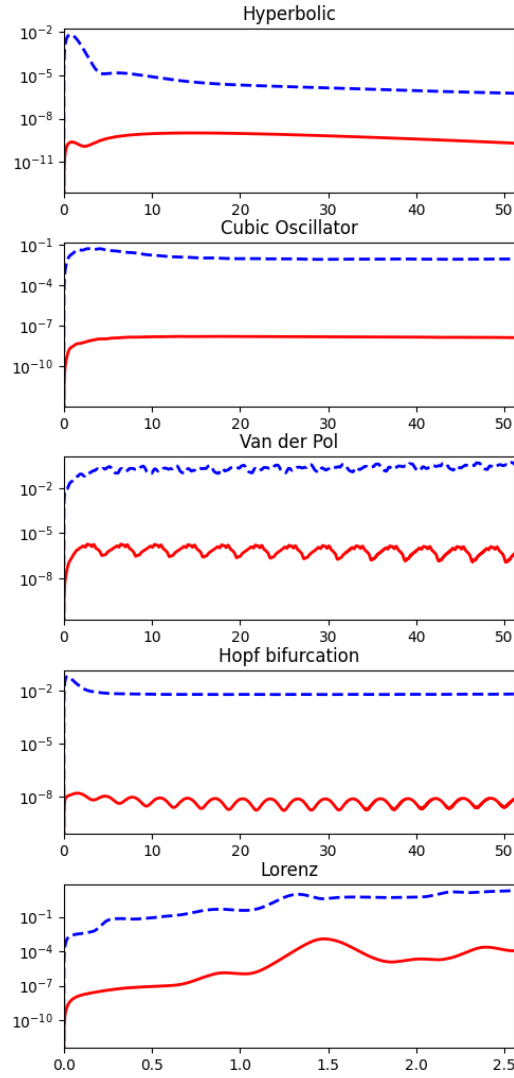


Figure 6: [nSINDy experiments] Time-instantaneous mean-squared errors. Two model are compared: the black-box neural ODE models (blue dashed lines) and the proposed neural SINDy model (red solid lines).

### Port-Hamiltonian structure preservation

Here, we consider the dictionary-based parameterization for the port-Hamiltonian systems. We follow the port-Hamiltonian neural network formulation presented in (Desai et al. 2021), which is written as:

$$\begin{bmatrix} \frac{dq}{dt} \\ \frac{dp}{dt} \end{bmatrix} = \begin{bmatrix} -\frac{\partial \mathcal{H}_\Theta}{\partial p} \\ \frac{\partial \mathcal{H}_\Theta}{\partial q} \end{bmatrix} + \begin{bmatrix} 0 \\ N \frac{\partial \mathcal{H}_\Theta}{\partial p} \end{bmatrix} + \begin{bmatrix} 0 \\ F(t) \end{bmatrix},$$

where  $\mathcal{H}_\Theta$  denotes the parameterized Hamiltonian function,  $N$  denotes the nonzero coefficient for a damping term, and  $F(t)$  denotes a time-dependent forcing. We consider the dictionary-type parameterization:

$$\mathcal{H}_\Theta = (\phi(q, p)^\top \Xi)^\top,$$

set  $N$  to be a trainable coefficient, and assume that  $F(t)$  is known.

As in (Desai et al. 2021), we consider the Duffing equation, where the Hamiltonian function is defined as

$$\mathcal{H}(q, p) = \frac{p^2}{2m} + \alpha \frac{q^2}{2} + \beta \frac{q^4}{4}.$$

With the Hamiltonian, the Duffing equation considering the damping term and the forcing can be written as:

$$\ddot{q} = -\alpha q - \beta q^3 + \gamma \sin(\omega t) - \delta \dot{q}.$$

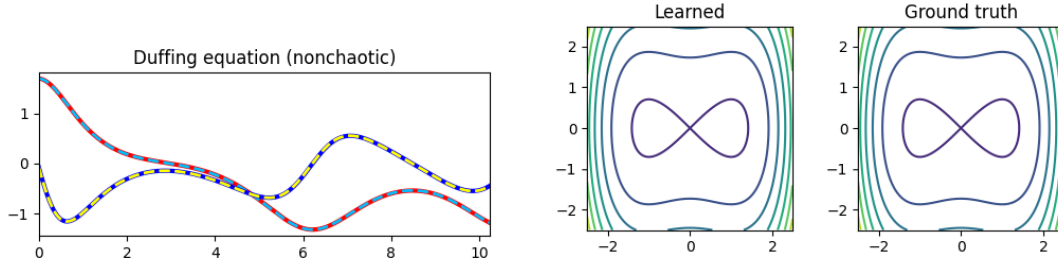


Figure 7: [Duffing equation] Left: Examples of reference trajectories (solid lines) and computed trajectories (dashed lines) from learned dynamics. Right: the learned and the ground truth Hamiltonian function evaluated on the uniform grid of  $(q, p)$ .

In the following experiment, we consider  $\mathcal{P}(2, 4) = \{1, q, p, q^2, qp, p^2, q^3, q^2pp^2, p^3, q^4, q^3p, q^2p^2, qp^3, p^4\}$  for parameterizing the Hamiltonian function.

**Nonchaotic case:**  $\alpha = -1, \beta = 1, \gamma = 0.3, \delta = 0.3$ , and  $\omega = 1.2$ . In the experiment, we assume that we know the values of  $\gamma$  and  $\omega$  and identify the Hamiltonian function. The identified Hamiltonian function is  $\mathcal{H}_\Theta(q, p) = 0.50015p^2 - 0.50004q^2 + 0.25010q^4$  and the identified value of  $\delta = 0.3002$ .

**Chaotic case**  $\alpha = -1, \beta = 1, \gamma = 0.1, \delta = 0.39$ , and  $\omega = 1.4$ . The identified Hamiltonian function is  $\mathcal{H}_\Theta(q, p) = 0.50007p^2 - 0.50053q^2 + 0.25017q^4$  and the identified value of  $\delta = 0.1001$ .